Numerical simulation of rock fragmentation during cutting by conical picks under confining pressure

Xuefeng Li[a], Shibo Wang[a,b,*], Shirong Ge[a,b] ,Reza Malekian[c], Zhixiong Li[a, d]

[a] School of Mechanical Engineering, China University of Mining and Technology, Xuzhou 221000, China

[b] Collaborative Innovation Center of Intelligent Mining Equipment, China University of Mining and Technology, Xuzhou 221000, China

[c] Department of Electrical, Electronic & Computer Engineering, University of Pretoria, Pretoria 0002, South Africa

[d] School of Mechanical and Manufacturing Engineering, UNSW Australia, Sydney 2052, Australia

Abstract: In this article, the effect of confining pressure on rock fragmentation process during cutting was investigated by numerical simulation with discrete element method (DEM). Four kinds of sandstones with different physical properties were simulated in the rock cutting models under different confining pressures. The rock fragmentation process, the cutting force and the specific energy under different confining pressures were analyzed. With the increase of confining pressure and rock strength, vertical propagation of cracks was restrained. Rock samples were compacted and strengthened by confining pressure resulting in the increase of the cutting force. The specific energy of rock cutting linearly increased with the increase of confining pressure ratio.

Key words: discrete element method; confining pressure; rock fragment; deep mine; conical pick.

1. Introduction

Much work has been done on the mechanism of rock fragmentation during rock cutting in the past decades. The classical theoretical models were proposed by Evans [1], Nishimatsu [2], and Niu [3] based on the maximum tensile stress theory, maximum-shear stress theory and fracture mechanics, respectively, which lead to better understanding on rock cutting process. However, it's difficult to predict cutting force effectively due to the anisotropy of rocks and the limitation of theoretical models. Besides, a lot of small-scale [4, 5] and full-scale [6-9] cutting tests have been carried out to study the effect of rock properties on cutting performance. Although experimental method is the most reliable and accuracy approach, it is time costly and expensive. Many scholars chose numerical simulation method to investigate the rock cutting process. Menezes et al. [10] performed the rock cutting simulation with a chisel pick using the explicit non-linear finite element method (FEM) software (viz., LS-DYNA). The effects of parameters such as rake angle, cutting velocity and cutting depth on the formation of discontinuous rock fragments were discussed. Zhou et al. [11] investigated the critical transition depth of failure mode during rock cutting process using LS-DYNA. Lei et al. [12] simulated the rock cutting process under hydraulic pressure using discrete element method (DEM) software in two dimensions (i.e. PFC2D). Huang et al. [13] study the transition of rock failure mode from ductile to brittle with the increase of cutting depth using PFC2D. Su et al. [14] built a rock cutting model using PFC3D and verified the reliable of this model in terms of cutting force prediction. Rojek [15] investigated the thermomechanical process during rock cutting and valuated the tool wear using DEM.

*Corresponding author：Tel: +86 516 83590709; fax: +86 516 83591916.
E-mail address: wangshb@cumt.edu.cn (Wang Shibo).

However, with an increasing demand for fossil energy, mining industries attempt to excavate for coal at an extreme depth, i.e., more than 1000 m [16]. The reserve of shallow mineral resources is decreasing and many mines have entered the 'deep mining' stage in China. The prominent difficulty of deep mining is the complex operation environment, namely high in-situ stress, high earth temperature, high water outburst pressure and strongly mining disturbance [17]. All these factors would result in high confining pressure on the rock/coal during the cutting process, which has significantly influence on the efficiency of the excavation/mining machines. In order to cut rock/coal securely and efficiently in deep mining, it is important to investigate the mechanism of rock fragmentation under high confining pressure condition. Much work has been done on the effect of confining pressure on rock indentation process with a cutter of tunnel boring machine (TBM). Gnirk et al. [18] conducted the rock indentation tests and found the transition of rock fracture mode from brittle to ductile as confining pressure increasing in rock indentation process. Chen et al. [19] observed two distinctive failure modes by examining different confinement/compressive strength ratios in rock indentation tests. Innaurato et al. [20], Yin et al. [21] and Huang et al. [22] found that thrust load increased in indentation tests with the increase of confining pressure and the fractures were more evidently directed towards the free edge under higher confining pressures. Ma et al. [23] conducted full-scale cutting tests to study the effect of confining pressure on TBM performance, and found that for the same cutting spacing and penetration, the normal force increases with the confining pressure due to enhancement of rock resistance strength and the confining pressure deviation between two confining directions has significant impact on TBM performance. Liu et al. [24-26] studied the rock breaking and chipping characteristics of TBM cutters under confining pressures by means of theoretical and experimental investigations. It was found that the chips were nearly rectangle shaped and the height decreased with increasing confining pressure. That means the confining pressure has important influence on the rock fragmentation process.

However, the relative movement between cutter and rock and the working condition are different excavation and mining. The movement of the pick can be simplified as linear cutting during mining with the rotation of shearer drum, while the movement between TBM disc cutter and rock is indentation. Fig. 1 shows the schematic of excavation and coal mining working face. It shows that the excavation process is kept in biaxial confining pressure condition, while the mining process is kept in uniaxial confining pressure condition. Bilgin et al. [27] studied the effect of confining pressure on cutting efficiency by numerical simulation and small-scale experiments with chisel picks and found that confining pressures dramatically decreased tensile stresses around the cutting groove and confining pressure caused an increase in cutting force around 20 or 30 percent more than unconfined conditions. Recently, Huang et al. [28] performed numerical simulations of rock cutting under confining pressures by FEM (LS-DYNA3D) and concluded that the cutting force increased with increasing confining pressures and the quality and particle size of chips were larger than that in unconfined condition. Li et al. [29] investigated the effect of confining pressure on rock cutting process by small-scale cutting tests and PFC2D, and found the transition of rock fracture from brittle to ductile with the increase of confining pressure. However, the effect of confining pressure on crack propagation and rock fragmentation during cutting with a conical pick has not been comprehensively explained. Hence, it's necessary to further investigate the effect of confining pressure on rock fragmentation process during cutting.

In this study, the numerical simulations of rock cutting with a conical pick were performed by PFC2D owning to its advantage in simulating the initiation and propagation of cracks. The reason for choosing PFC2D but not PFC3D or LS-DYNA3D in the investigation can be explained as follows. To the best of our knowledge, there are two main aspects that the numerical simulation concerns. One is cutting force prediction and the other is full understanding of the cutting mechanism. The numerical technique in 3D (LS-DYNA3D or PFC3D) is more advanced in force prediction while the PFC2D is sophisticated in the

simulation of the initiation and propagation of cracks, which would be helpful for full understanding the mechanism of rock cutting process. Comparing the simulation results of PFC2D, PFC3D (Su et al. [14]) and LS-DYNA3D (Huang et al. [28]) in the rock cutting simulation, it can be noticed that the PFC2D reveals the propagation of rock cracks but its application is limited in predicting the cutting force, which can be solved by the PFC3D or LS-DYNA3D. However, the PFC3D or LS-DYNA3D does not provide better details than PFC2D on the crack propagation. In addition, the computation of PFC3D and LS-DYNA3D is time-consumed. Because our aim is to investigate the initiation and propagation of the rock cracks during cutting process, it is reasonable to employ PFC2D for this purpose. In the PFC2D simulations, the DEM models of four kinds of sandstones with different physical properties were calibrated and cut under different confining pressures. The effects of confining pressure on rock fragmentation process, cutting force and specific energy were analyzed.

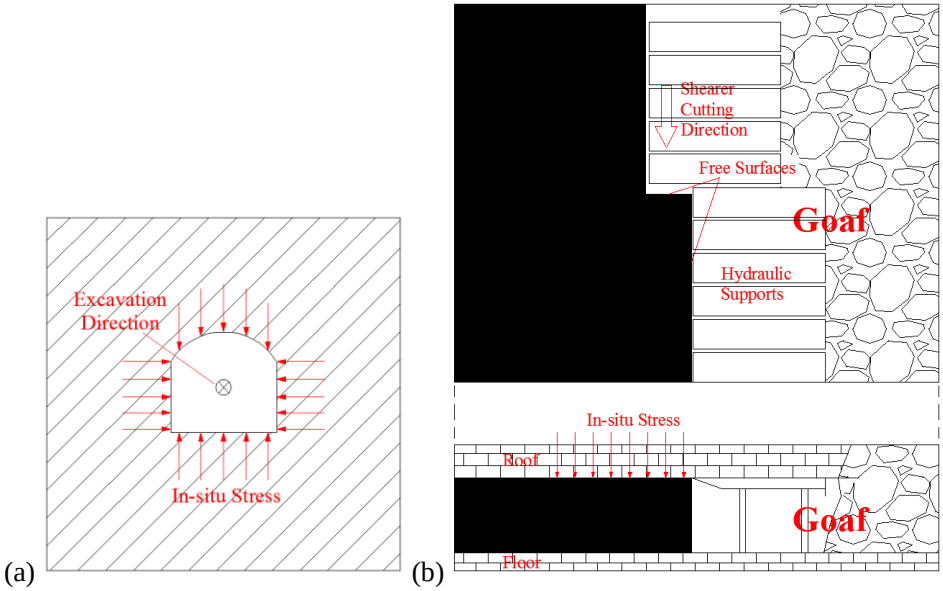

(a) (b)

Fig. 1. Schematics of (a) excavation and (b) coal mining working face.

2. Model establishment and calibration

In order to investigate the rock fragmentation with a conical pick in confining conditions, a DEM model was established in this work for numerical evaluations under different confining pressures. The micro-properties of rock samples were calibrated. The strength and deformability properties of the rocks with different modulus ratios according to Deere and Miller [30] were inspected in the numerical analysis.

2.1. Basic theory of PFC

PFC is a commercial DEM-software which is widely used in solving rock mechanics problems. The DEM models in PFC are established by particles and the particle assembly flows to an equilibrium state in the simulation. The aim of PFC simulation is to find the equilibrium state that alternates between Newton's second law and a force-displacement law in the DEM models [31]. Newton's second law gives the motion of particles and the force-displacement law is used to find the force from relative displacement between particles or particle and wall. The force, motion and location of particles and walls are updated every cycle during simulation.

In this study, the linear parallel bond model is applied to contacts between particles as it can restrict both sliding and rotation between particles. In PFC, contact bonds are the medium translating force and

movement between particles and are described as gluing particles together via restricting sliding or rotation. When the contact stresses exceed the tensile or shear strength, the bond breaks. The initiation and propagation of cracks can be represented explicitly in PFC as broken bonds.

The total force and moment associated with the *i*th parallel bond are denoted by $\overline{F}_i$ and $\overline{M}_i$ as shown in Fig. 2. The vector of $\overline{F}_i$ is resolved into normal and shear components with respect to the contact plane as described in Eq. (1) [31].

$$\overline{F}_i = \overline{F}_i^n + \overline{F}_i^s \tag{1}$$

where $\overline{F}_i^n$ and $\overline{F}_i^s$ denote the normal and shear component vectors, respectively. When the bond forms, $\overline{F}_i$ and $\overline{M}_i$ are initialized to zero.

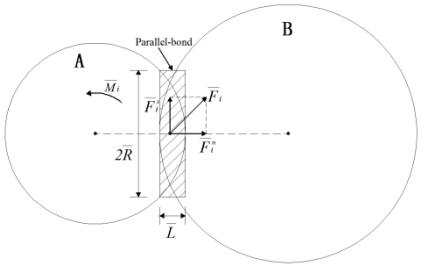

Fig. 2. Schematic of the parallel bond in PFC [31].

Each subsequent relative displacement and rotate-increment at the contact results in an increment of elastic force and moment which are added to the current values. Eq. (2)-(4) describe their updating process.

$$\overline{F}_i^n = \overline{F}_i^n - k^n A \Delta U_i^n \tag{2}$$

$$\overline{F}_i^s = \overline{F}_i^s - k^s A \Delta U_i^s \tag{3}$$

$$\overline{W}_i = \overline{W}_i - k^n I \Delta \theta_i \tag{4}$$

$$\text{with } \Delta U_i = V_i \cdot t,\ \Delta \theta_i = (\omega_i^B - \omega_i^A) \cdot t,\ A = 2\overline{R},\ I = \frac{2}{3}\overline{R}^3$$

where Δ is a symbol of increment; ΔU_i is the relative displacement between the bonded particles in one time step, and superscripts *n* and *s* denote its normal and shear components, respectively; *t* is the time step; V_i is the relative velocity between the bonded particles; $\Delta\theta_i$ is the relative rotation angle between the bonded particles; ω^A and ω^B are angular velocities of the bonded particles; *A* is the area of the bond disk; *I* is the moment of inertia of the disk cross-section about an axis through the contact point and in the direction of $\Delta\theta_i$; $\overline{R}$ is the parallel-bond radius; k^n and k^s are the normal and shear contact stiffness, respectively.

2.2. Calibration of rock sample

Coal fields are formed due to sedimentary movement in geologic history and most surrounding rocks are sedimentary rocks [32], such as sandstone, limestone, dolostone and shale. The sandstone is among the most pervasive rock type. In order to investigate the effect of confining pressure on fragmentation of rocks, four types of sandstone were selected according to Deere and Miller's engineering classification of rocks in different strength and modulus ratio levels marked with yellow stars shown in Fig.3. Rock samples of S1, S2 and S4 locate in low, medium and high strength levels, respectively, with average modulus ratio of approximately 300 and S3 is medium strength sandstone with low modulus ratio of 150. The modulus ratio is the ratio to Young's modulus to uniaxial compressive strength (UCS) of the rock. In order to investigate

the sensitivity of rock properties to confining pressure, S2 and S3 have the same UCS but different Young's modulus, and S1, S3 have the same Young's modulus but different UCS. The mechanical properties of rocks are listed in Tab.1. The micro parameters of particle assemblies for the four sandstones are given in Tab.2, where the particle assemblies were calibrated by UCS simulation tests.

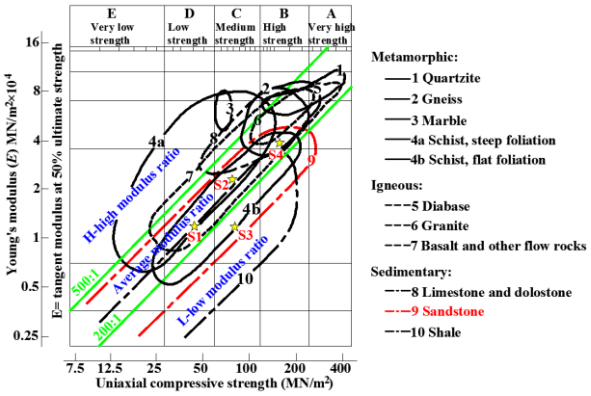

Fig.3. Deere and Miller's engineering classification of rocks taken from Bell [33] with four typesof sandstone calibrated marked on.

2.3. Establishment of models

Referring to Fig. 1(b), before cutting operation, only the goaf-side of working face is free and the coal seam is in biaxial compressive state. With the advance of shearer, the in-situ stress acting on the coal at the working face changes from biaxial compressive state to uniaxial compressive state, which is mainly composed of the gravity of overlying strata. Fig. 4 shows the schematic of rock cutting model under confining pressure. The schematic of mining with a shearer in the working face is shown in Fig. 4(a). The motion of the pick is simplified as linear and the in-situ stress is simplified along the cutting velocity of the pick. The rock sample is created with dimensions of 100×200 mm including 73889 particles. In order to decrease the computing time, the rock sample is graded by particle radius with upper layer radii of 0.1~0.3 mm and bottom layer radii of 0.3~0.5 mm drawn from uniform distribution. Fig. 4(b) shows the compressive process before cutting. When the bonded particle assembly approaches to an equilibrium state, the walls in two directions are servo controlled to exert load to the magnitude of in-situ stress. Afterwards, the upper wall is deleted regarded as the free surface in the shearer cutting direction and the confining pressure keeps being a constant in horizontal direction loaded by lateral walls as shown in Fig. 4(a). Meanwhile, a 2D conical pick is imported with a certain rake angle and cutting depth as illustrated in Fig. 4(a). In the simulation, in order to prevent the interference between the body of pick and rock, the rake angle was set to be 55°. The cutting depth was set to be 6 mm which is larger than 20 times of the radii of upper layer particles (0.1~0.3 mm).

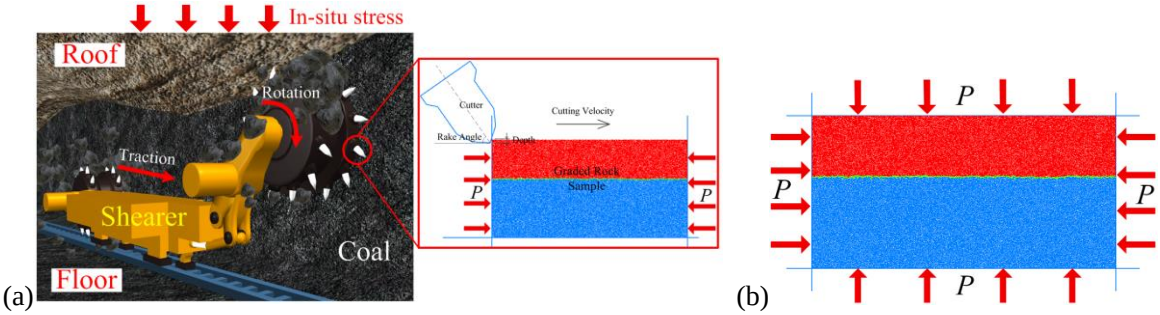

(a) (b)

Fig. 4. Schematic of rock cutting model under confining pressure.

2.4. Selection of confining pressure

The confining pressure may influence the rock fragmentation process and the performance of mining machinery. However, it should be noted that there is not a clear classification for the issue of confining pressure for rock cutting. According to reference [34], the effect of confining pressure on rock physical properties varies with different rock types. In the simulation, the four sandstones with different UCS ranging from 40 to 134 MPa were cut under a wide range of confining pressures. Tab.3 lists the simulation parameters, where λ is the ratio of confining pressure to UCS.

3. Results and discussions

3.1. Effect of confining pressure on rock fragmentation

Fig. 5 shows the fragmentation process of S1 under confining pressure of 5 MPa. As the pick advancing, a crushed zone was formed ahead the pick tip in which bonds between particles were almost broken. Then cracks initiated beneath the pick and propagated to the free surface along a concave-upward curve to produce rock chips. Besides, some cracks propagated vertically without chip formation. Afterwards, a serials of similar chip formation processes occurred with increasing the cutting distance *l*. Videlicet, the rock fragmentation process is a cyclic process during cutting.

Fig. 6 shows the fragmentation of different sandstones under different confining pressures. Chips are illustrated in different colors and cracks are shown as red and green segments regarding as tensile cracks and shear cracks, respectively. Fig. 6(a) shows the fragmentation of S1 under different confining pressures. When the confining pressure ratio was 0 MPa, the cut surface was very irregular with chips produced beneath the pick tip. However, with the increase of the confining pressure ratio, cracks propagated horizontally and vertical cracks were restrained which resulted in the cut surface tending to be smooth. As the confining pressure increasing, the criterion for the vertical crack initiation can only be met at a larger depth in rock indentation and the point of the maximum tensile stress, at which the cracks initiate, moves away from the indentation axis and tends to be closer to the free surface [35]. Indeed, for a large enough confining pressure, e.g. λ=0.5, the stress beneath the pick may even become compressive. Fig. 6(b)-(d) show fragmentation of S2, S3 and S4 with confining pressure ratios of 0, 0.375 and 0.6, and similar effects of confining pressure on rock fragmentation of different rocks were observed. Besides, for rocks with different UCS in unconfined condition (shown as a1, b1, c1 and d1 in Fig. 6), the formation of rock chips beneath the pick and vertical crack propagation tended to be restrained when the UCS of rock increased with the same cutting depth. It is suspected that the high strength of rock suppresses crack propagation and the cutting depth is not large enough to induce vertical cracks in high strength rocks.

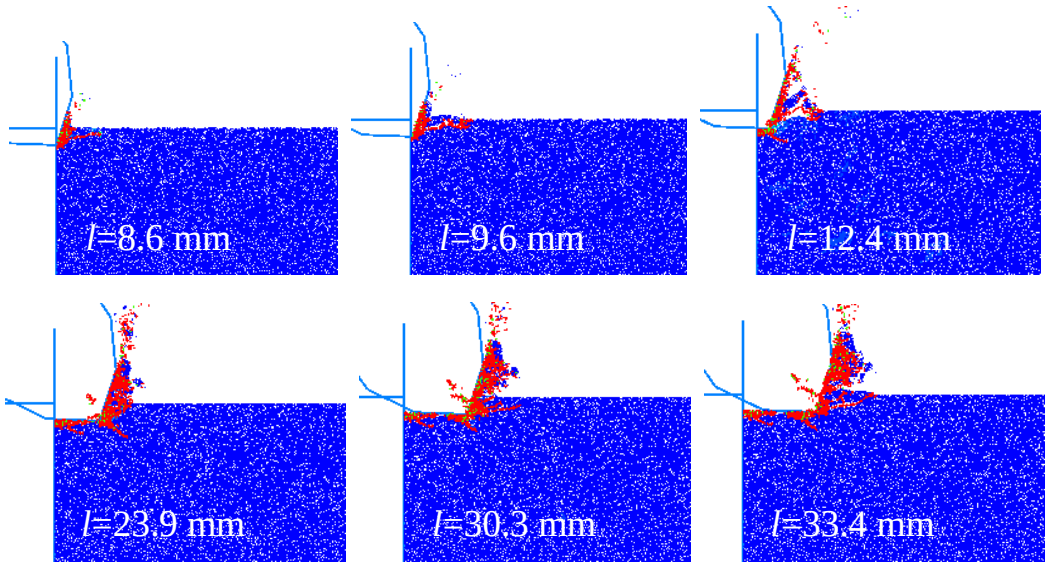

Fig. 5. Fragmentation process of S1 under confining pressure of 5 MPa.

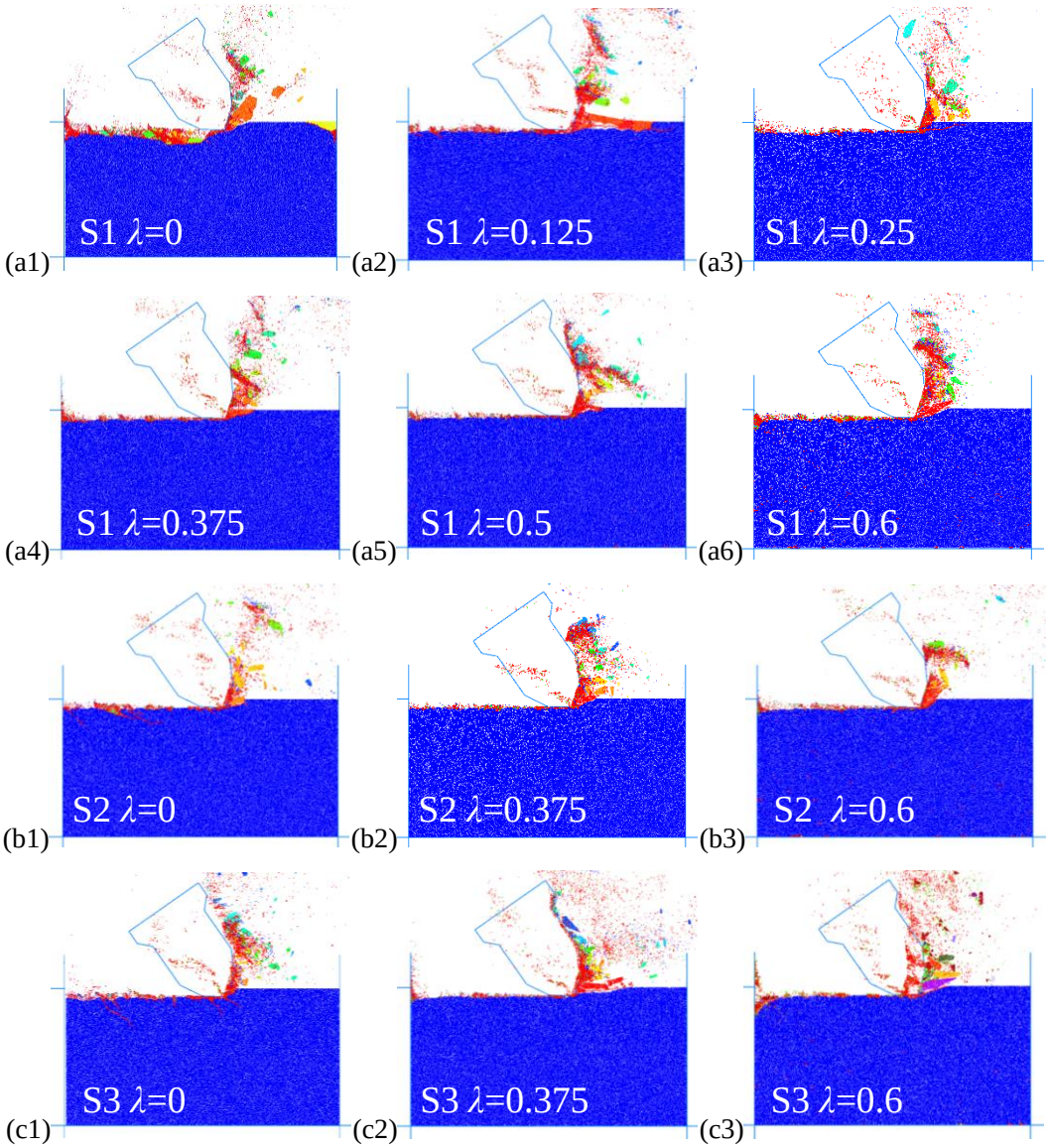

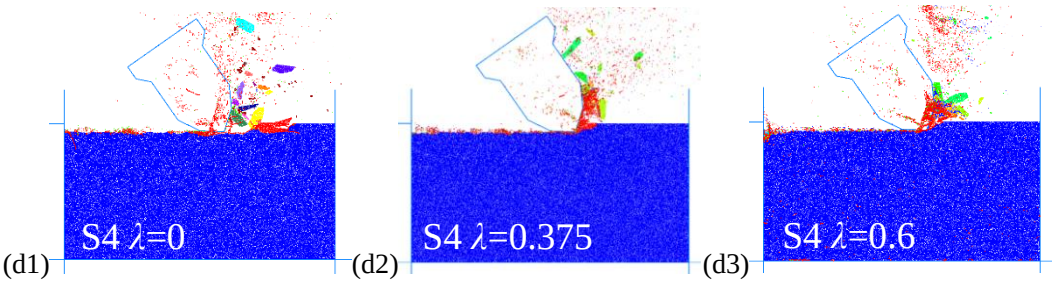

(d1) (d2) (d3)

Fig. 6. Fragmentation of (a) S1, (b) S2, (c) S3 and (d) S4 under different confining pressures.

Fig. 7 shows the contact force distribution between particles during cutting on S1. The black and saffron segments are compressive and tensile forces, respectively, and the width of the segment represents the amplitude of the contact force. In the condition of unconfined (Fig. 7a), there are little residual contact forces between particles across the rock sample. During the cutting process, a crash zone beneath the tip of the pick is formed with compressive stress concentration. Micro tensile fractures (red segments in Fig. 7) are formed in the crash zone and combined to be a macro crack. The macro crack is almost perpendicular to the rake of the pick. At the end of the macro crack, there is a crack propagation zone with tensile stress concentration. The macro cracks propagated in tensile failure in unconfined cutting condition. Different from the unconfined condition, shear (green segments) and tensile (red segments) cracks are formed in the crash zone beneath the pick tip shown in Fig. 7b in the confined cutting condition. The macro tensile cracks propagate almost horizontally outside the crash zone. This is because that the tensile contact forces are vertical due to the horizontal compressive contact forces between particles outside the crash zone in the confined condition. Consequently, the cracks are formed in shear and tensile failure in the crash zone, and propagate primarily in tensile failure during cutting in confined condition.

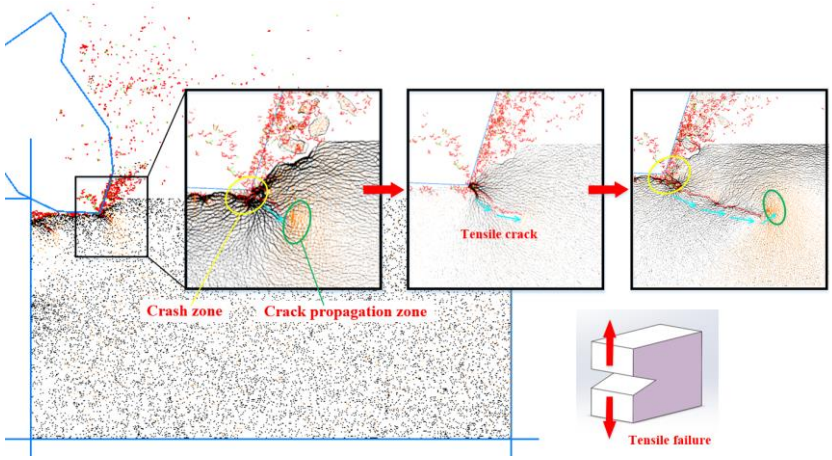

(a)

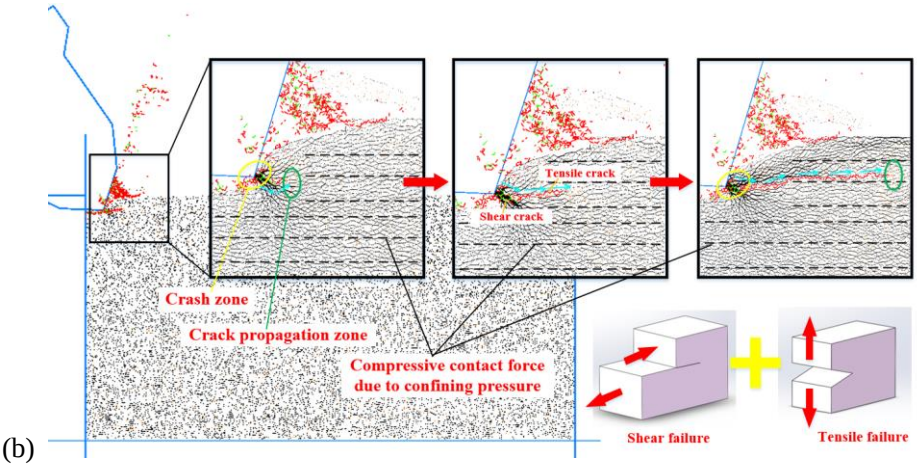

(b)

Fig. 7. Contact stress distribution during cutting on S1: (a) unconfiend, (b) with a confining pressure ratio of 0.375

3.2. Effect of confining pressure on cutting force

Fig. 8 shows the cutting force variation of different rocks with confining pressure ratio of 0.375. It shows that the cutting force oscillates as saw-teeth during the cutting process. The upward stage of the curve represents that the pick penetrates into the rock and the cutting force increases with the increase of penetration length. Meanwhile, a crush zone is formed and micro fractures combined as macro cracks to form rock chips. As chip being formed, the contact between pick and rock disappears, resulting in the abrupt drop of cutting force. When the pick is advancing, the cutting force fluctuates with the formation of chips.

Fig. 9 shows the relationship between confining pressure ratio and mean peak cutting force and mean cutting force of different rocks. Both the mean force and the mean peak force increase with the increase of confining pressure, for instance, the mean peak cutting forces with confining pressure ratio of 0.6 are larger than those unconfined by 80%, 32.9%, 42.5% and 93.4% for S1, S2, S3 and S4, respectively. As shown in Fig. 9, the magnitude of cutting force is mainly determined by the UCS of rock and confining pressure. The mean peak cutting force is much larger than mean cutting force, and accordingly, the mean peak cutting force is a more reasonable parameter in evaluating the working state of the pick and designing excavation equipments. The mean peak cutting force with the cutting depth of 6 mm can be expressed as Eq. (5) by multiple element linear regression with R^2 = 0.9287 shown in Fig. 10.

$$F_C' = 172.18\lambda + 2.82\sigma_c - 51.99 \tag{5}$$

where F_C' is the mean peak cutting force (kN), λ is confining pressure ratio, and σ_C is the UCS of rock (MPa). According to Eq. (5), there is a linear relationship between mean peak cutting force and UCS of rock in the condition of a certain confining pressure ratio which is in consistent with the results obtained from unconfined linear rock cutting tests in reference [36]. However, the Young's modulus has little influence on the mean peak cutting force according to the comparison between S2 and S3.

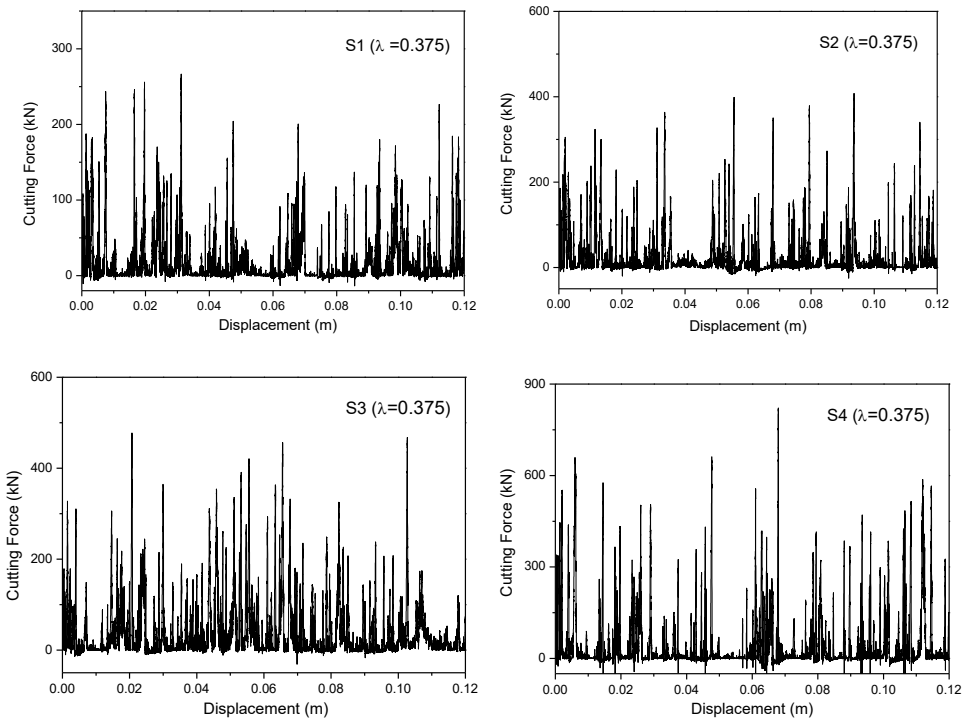

Fig. 8. Cutting force variation of different rocks with confining pressure ratio of 0.375.

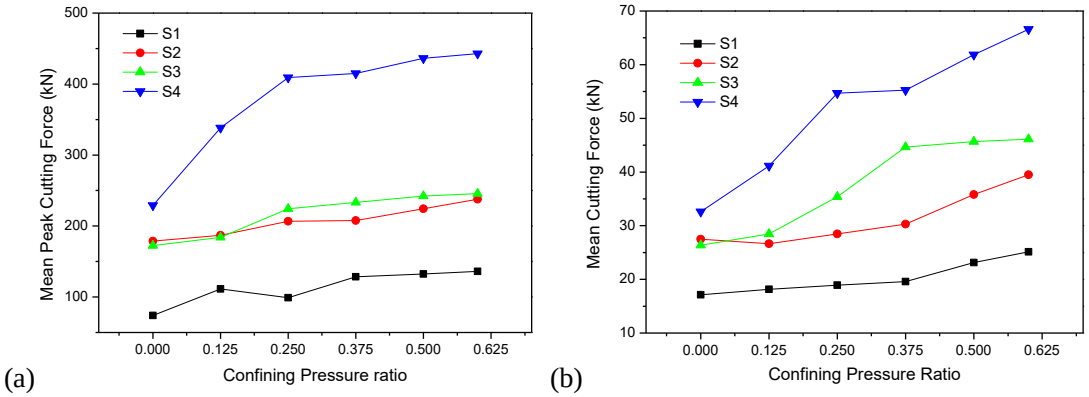

(a) (b)

Fig. 9. Relationships between confining pressure ratio and (a) mean peak cutting force, (b) mean cutting force.

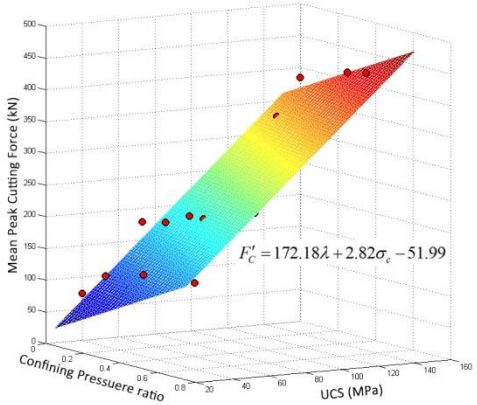

Fig. 10. Relationship between mean peak cutting force and confining pressure ratio and UCS.

Fig. 11 shows the variation of cumulative fracture numbers of S1 and S4 during cutting process under

different confining pressures. As the pick advancing, the cumulative fracture number increases with stairs due to rock chip formation. The types of fracture include shear fracture and tensile fracture. Evidently, the cumulative number of tensile fractures is much higher than that of shear fractures. This indicates that the fractures in rock cutting are mainly tensile fractures. Besides, the quantity ratios of shear to tensile fractures at the end of cutting process for different rocks were calculated. The relationship between confining pressure ratio and the quantity ratio of shear to tensile fractures is shown in Fig. 12. It shows that the quantity ratio of shear to tensile fractures increases with the increase of confining pressure ratio. According to Fig. 8, the shear fracture mainly appears in the crush zone. It indicates that with the increase of confining pressure ratio, the fragmentation is severer in the crush zone and the crack propagation tends to be more difficult. However, the effect of rock properties on the quantity ratio of shear to tensile fracture is unobvious.

Moreover, the mean contact force between particles was calculated after the rock sample being compacted under a certain confining pressure. Fig. 13 shows the relationship between mean contact force and confining pressure. The mean contact force increases linearly with the increase of confining pressure with a high correlation coefficient of 1. It indicates that the mean contact force between particles is determined by confining pressure. Since the tensile fracture is the main fracture type of rocks during cutting process, the cutting force should firstly overcome the compressive contact force between particles, and then the cutting force further increases to break the bonds between particles in tensile failure mode. Afterward, micro fractures are combined into macro cracks and propagate to the free surface to form rock chips. The increasing of cutting force with the increase of confining pressure mainly induced by the higher contact force between particles in high confining pressure. Namely, rock samples were compacted and strengthened by confining pressure.

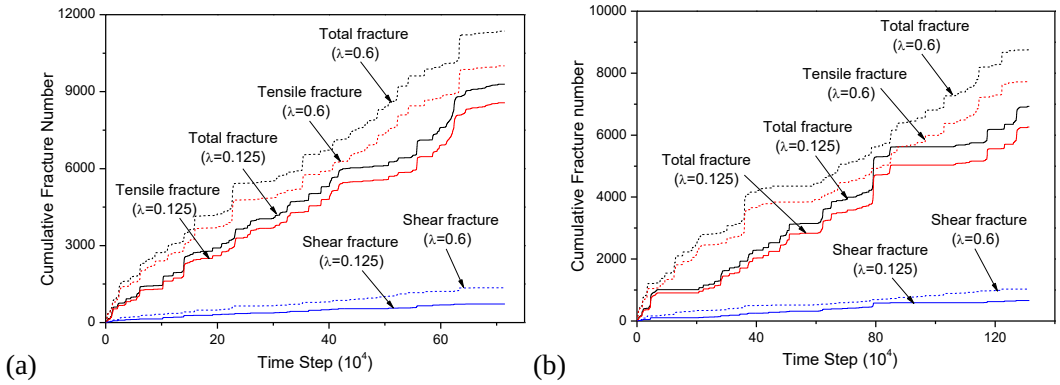

Fig. 11. The variation of cumulative fracture numbers during cutting (a) S1 and (b) S4 under different confining pressures.

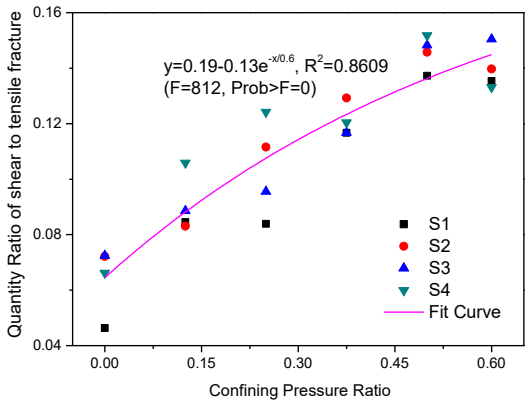

Fig. 12 The relationship between confining pressure ratio and the quantity ratio of shear to tensile fractures

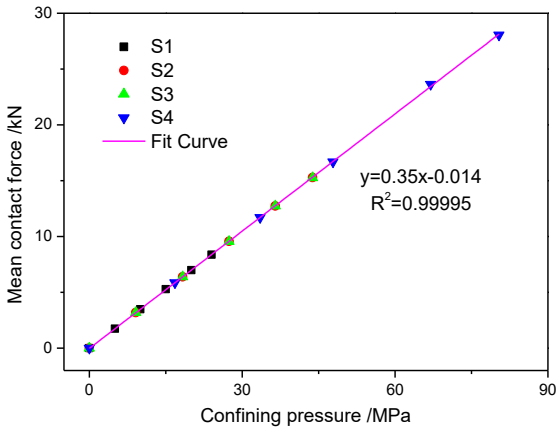

Fig. 13. The relationships between confining pressure and mean contact force

3.3. Effect of confining pressure on specific energy

Specific energy (SE) is defined as the amount of work required breaking a unit volume of rock and is widely used to evaluate the performance of mining and excavation machinery [37]. *SE* is calculated as Eq. (6).

$$SE = \frac{W}{V_C} = \frac{\int_0^l F_C dx}{V_C} \tag{6}$$

where W is the work done by the pick (MJ/m^3) calculated by integrating cutting force (F_C) on cutting length, and V_C is the total volume of chips calculated by summing the volume of particles separated from the rock block.

Fig. 14 shows the relationships between confining pressure ratio and SE of different rocks. For each rock sample, SE increased linearly with the increase of confining pressure ratio. Furthermore, SE increased with the increase of UCS of rocks. Since the confining pressure strengthens the rock strength analyzed above, SE has a negative relationship with rock strength which is in consistent with the conclusion obtained from full-scale rock cutting tests [37]. Moreover, the slop of SE vs confining pressure ratio increased with the increase of rock UCS. This means that the cutting efficiency of rocks with high strength is more sensitive to confining pressure ratio than rocks with lower strength.

The size distribution of rock chip has significant impact on SE, and it follows a reverse trend to SE [38]. In order to quantitatively evaluate the size of rock chips in PFC, specific chip volume (SCV) is proposed as the chip volume produced by forming unit length of crack calculated by Eq. (8).

$$SCV = \frac{V_C}{L} \tag{8}$$

where L is the total length of cracks produced during cutting. The smaller value of SCV indicates that smaller rock chips are produced.

Fig. 15 shows the relationships between confining pressure ratio and SCV of different rocks. With the increase of confining pressure, SCV decreases rapidly at first and then tends to be a constant at the confining pressure ratio of approximately 0.375. Hence, as analyzed above, it is probably that the increase of cutting force and the decrease of the size of rock chips induced by confining pressure are the main reason for the increase of SE.

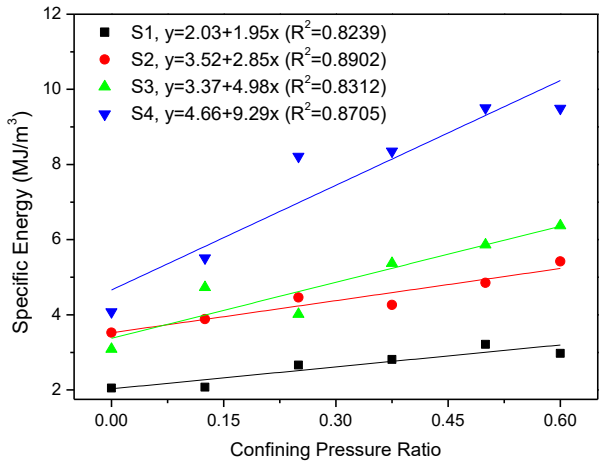

Fig. 14. Relationships between confining pressure ratio and SE.

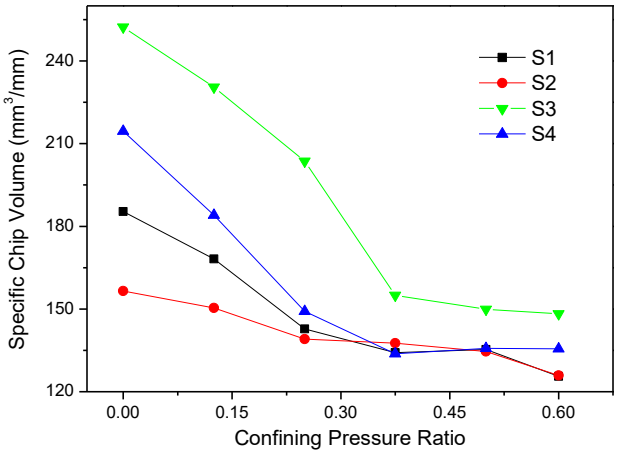

Fig. 15. Relationships between confining pressure ratio and SCV.

4. Conclusion

The numerical evaluation of rock cutting with a conical pick under different confining pressures have been conducted to investigate the effect of confining pressure on rock fragmentation and cutting behavior in this paper. The findings can be concluded as follows:

(1) The rock cutting process was a cyclic process with rock chips formation. In one cycle, a crush zone was formed near the pick tip firstly, and then cracks initiated beneath the pick tip and propagated to the free surface along a concave-upward curve to produce rock chips. With the increase of confining pressure and rock strength, vertical propagation of cracks was restrained.

(2) Fractures were mainly formed in tensile failure mode and rock samples were compacted and strengthened by confining pressure, which resulted in the increase of the mean peak cutting force and mean cutting force. A linear positive correlation between the mean peak cutting force, the UCS of rock, and confining pressure ratio was obtained by multiple element linear regression with a high correlation coefficient of 0.9287.

(3) The specific energy of rock cutting linearly increased with the increase of confining pressure ratio due to the increase of cutting force and the decrease of the size of rock chips. In addition, the efficiency in cutting rocks with high strength is more sensitive to confining pressure ratio than that with low strength.

Acknowledgements

This research was supported by the National Basic Research Program of China (2014CB046301), the National Natural Science Foundation of China (U1510116, 51304190), the Key Program of Shanxi Coal Basic (MJ2014-05), the Science and Technology Project of Jiangsu Province (BK20140051), a Project Funded by the Priority Academic Program Development of Jiangsu Higher Education Institutions (PAPD).

Reference

[1] I. Evans, A theory of the picks cutting force for point-attack, Int. J. Min Eng. 2(1) (1984) 63-71.

[2] Y. Nishimatsu, The mechanics of rock cutting, International Journal of Rock Mechanics and Mining Sciences & Geomechanics Abstracts, Pergamon, 9(2) (1972) 261-270.

[3] D.M. Niu, Mechanical model of coal cutting, J. China Coal Soc. 19(5) (1994) 526–529.

[4] R.J. Fowell, I. McFeat-Smith, Factors influencing the cutting performance of a selective tunnelling machine, Proceedings of tunnelling symposium 76(1976) 301-309.

[5] I. McFeat-Smith, R.J. Fowell, The selection and application of roadheaders for rock tunneling, Proceedings of the Rapid Excavation and Tunnelling Conference, Atlanta, 1(1979) 261-279.

[6] A.W. Khair, Design and fabrication of a rotary coal cutting simulator, Proceedings of the Coal Mine Dust Conference, 1984. pp. 190-197.

[7] B. Asbury, M. Cigla, C. Balci, Design methodology, testing and evaluation of a continuous miner cutterhead for dust reduction in underground coal mining, SME Annual Meeting, Phoenix, Arizona, 2002. pp. 1-8.

[8] C. Balci, D. Tumac, Investigation into the effects of different rocks on rock cuttability by a V-type disc cutter, Tunn. Undergr. Sp. Tec. 30(2012) 183-193.

[9] M.Z.A. Bakar, L.S. Gertsch, Evaluation of saturation effects on drag pick cutting of a brittle sandstone from full scale linear cutting tests, Tunn. Undergr. Sp. Tec. 34(2013) 124-134.

[10] P.L. Menezes, M.R. Lovell, I.V. Avdeev, J.S. Lin, C.F. Higgs III, Studies on the formation of discontinuous chips during rock cutting using an explicit finite element model, Int. J. Adv. Manuf. Tech. 70(2014) 635-648.

[11] Y. Zhou, J.S. Lin, On the critical failure mode transition depth for rock cutting, Int. J. Rock Mech. Min. Sci. 62(2013) 131-137.

[12] S.T. Lei, P. Kaitkay, Distinct element modeling of rock cutting under hydrostatic pressure, Key Engineering Materials, 250(2003) 110-117.

[13] H. Huang, B. Lecampion, E. Detournay, Discrete element modeling of tool-rock interaction I: rock cutting, International Journal for Numerical and Analytical Methods in Geomechanics, 37(13)(2013) 1913-1929.

[14] O. Su, N.A. Akcin, Numerical simulation of rock cutting using the discrete element method, Int. J. Rock Mech. Min. Sci. 48(3) (2011) 434-442.

[15] J. Rojek, Discrete element thermomechanical modelling of rock cutting with valuation of tool wear, Computational Particle Mechanics, 1(1) (2014) 71-84.

[16] N. Zhang, X.Y. Li, X.G. Zheng, F. Xue, The status of deep coal mine and technical challenges, National Technology Conference of Kilometers Deep Coal Mine, Taian, 2013.

[17] M.C. He, Conception system of deep and evaluation index for deep engineering, ISRM International Symposium-Eurock 2005, ISRM, 2005.

[18] P.F. Gnirk, J.B. Jr, An experimental study of single bit-tooth penetration into dry rock at confining pressures 0 to 5,000 psi, Soc. Petrol Eng. J. 5(2) (1965) 117-130.

[19] L.H. Chen, J.F. Labuz, Indentation of rock by wedge-shaped tools, Int. J. Rock Mech. Min. Sci. 43(7) (2006) 1023-1033.
[20] N. Innaurato, C. Oggeri, P.P. Oreste, R. Vinai, Experimental and numerical studies on rock breaking with TBM tools under high stress confinement. Rock Mech. Rock Eng. 40(5) (2007) 429-451.
[21] L.J. Yin, Q.M. Gong, H.S. Ma, J. Zhao, X.B. Zhao, Use of indentation tests to study the influence of confining stress on rock fragmentation by a TBM cutter. Int. J. Rock Mech. Min Sci. 72 (2014) 261-276.
[22] H. Huang, E. Detournay, Discrete element modeling of tool-rock interaction II: rock indentation, Int. J. Numer. Anal. Met. 37 (13) (2013) 1930-1947.
[23] H.S. Ma, Q.M. Gong, J. Wang, L. Yin, X.B. Zhao, Study on the influence of confining stress on TBM performance in granite rock by linear cutting test, Tunn. Undergr. Sp. Tec. 57 (2016) 145-150.
[24] J. Liu, P. Cao, K. Li, A study on isotropic rock breaking with TBM cutters under different confining stresses, Geotech. Geol. Eng. 33 (6) (2015) 1379-1394.
[25] J. Liu, P. Cao, J. Liu, Z. Jiang, Influence of confining stress on fracture characteristics and cutting efficiency of TBM cutters conducted on soft and hard rock, J. Cent. South Univ. T. 22 (2015)1947-1955.
[26] J. Liu, P. Cao, Study on Rock Fracture with TBM Cutter under Different Confining Stresses, I. G. J. 46 (1) (2016) 104-114.
[27] N. Bilgin, H. Tuncdemir, C. Balci, H. Copur, S. Eskikaya, A model to predict the performance of tunneling machines under stressed conditions, Proceedings of the AITES-ITA 2000 World Tunnel Congress, Durban, Published by The South African Institute of Mining and Metallurgy, Johannesburg, Republic of South Africa, May, 2000. pp. 13-18.
[28] J. Huang, Y. Zhang, L. Zhu, T. Wang, Numerical simulation of rock cutting in deep mining conditions, Int. J. Rock Mech. Min. Sci. 84 (2016) 80-86.
[29] X.F. Li, S.B. Wang, R. Malekian, S.Q. Hao, Z.X. Li, Numerical Simulation of Rock Breakage Modes under Confining Pressures in Deep Mining: An Experimental Investigation. IEEE Access, 4(2016) 5710-5720.
[30] Deere DU, Miller RP. Engineering classification and index properties for intact rock. Air Force Weapons Lab: Kirtland Air Base. New Mexico; 1966.
[31] Itasca Consulting Group Inc. PFC2D/3D (Particle Flow Code in2/3 Dimensions), Version 5.0. Minneapolis. MN: ICG, 2014.
[32] M.G. Qian, P.W. Shi, J.L. Xu, Mining pressure and strata control, China University of Mining and Technology Press, Xuzhou, 2003.
[33] F.G. Bell, Engineering properties of soils and rocks, Cohesive Soils 48 (4) (1981) 416-417.
[34] Y.J. Yang, Y. Song, S.J. Chen, Test study of coal's strength and deformation characteristics under triaxial compression, J. China Coal Soc. 31 (2) (2006) 151-153.
[35] H. Huang, B. Damjanac, E. Detournay, Numerical modeling of normal wedge indentation in rocks with lateral confinement, Int. J. Rock Mech. Min. Sci. 34 (3–4) (1997) 81-94.
[36] N. Bilgin, M.A. Demircin, H. Copur, et al, Dominant rock properties affecting the performance of conical picks and the comparison of some experimental and theoretical results, Int. J. Rock Mech. Min. Sci. 43(1) (2006) 139-156.
[37] C. Balci, M.A. Demircin, H. Copur, H. Tuncdemir, Estimation of optimum specific energy based on rock properties for assessment of roadheader performance, J. S. Afr. I. Min Metall. 11 (2004) 633-642.
[38] H.S. Ma, Q.M. Gong, J. Wang, X.B. Zhao, L.J. Yin, C.T. Miao, G.W. He, Linear cutting tests on effect of confining stress on rock fragmentation by TBM cutter, Chinese J. Rock. Mech. Eng. 35 (2016) 346-355.

Tab.1 Properties of simulated sandtones

Rock materials		UCS/MPa	*E*/GPa	Modulus ratio	μ
Low strength	S1	40	12	300	0.24
Medium strength	S2	73	23	315	0.24
	S3	73	11	150	0.24
High strength	S4	134	40	298	0.24

where UCS is the uniaxial compressive strength, E is the Young's modulus, μ is the Poisson's ratio.

Tab.2 Micro parameters and macro properties of sandstone models

Properties	S1		S2		S3		S4	
Paricle radius/mm	0.1-0.3	0.3-0.5	0.1-0.3	0.3-0.5	0.1-0.3	0.3-0.5	0.1-0.3	0.3-0.5
Bond elastic modulus/GPa	6.18	6.18	12	12	5.78	5.78	21	21
Bond stiffness ratio	2.1	2.1	2.1	2.1	2.1	2.1	2.1	2.1
Bond tensile strength/MPa	16	15.6	29.5	29	29.3	29.3	54	5.22
Bond shear strength/MPa	16	15.6	29.5	29	29.3	29.3	54	5.22
Particle elastic modulus/GPa	6.18	6.18	12	12	5.78	5.78	21	21
Particle stiffness ratio	2.1	2.1	2.1	2.1	2.1	2.1	2.1	2.1
UCS/MPa	39.4	40.1	73.8	73.16	73.04	72.84	133.97	133.86
E /GPa	11.9	11.8	23.2	22.9	11.16	11.02	40.57	40
μ	0.245	0.234	0.245	0.234	0.245	0.235	0.245	0.234

Tab.3. Confining pressures assigned for the four sandstones.

Rock type	UCS/MPa	Confining pressure/MPa	λ
S1	40	0, 5, 10, 15, 20, 24	0, 0.125, 0.25, 0.375, 0.5, 0.6
S2, S3	73	0, 9.1, 18.3, 27.4, 36.5, 43.8	0, 0.125, 0.25, 0.375, 0.5, 0.6
S4	134	0, 16.8, 33.5, 47.8, 67, 80.4	0, 0.125, 0.25, 0.375, 0.5, 0.6